nature ecology & evolution

ARTICLES

https://doi.org/10.1038/s41559-019-0993-0

Single nucleotide mapping of trait space reveals Pareto fronts that constrain adaptation

Yuping Li[1], Dmitri A. Petrov[1*] and Gavin Sherlock[2*]

Trade-offs constrain the improvement of performance of multiple traits simultaneously. Such trade-offs define Pareto fronts, which represent a set of optimal individuals that cannot be improved in any one trait without reducing performance in another. Surprisingly, experimental evolution often yields genotypes with improved performance in all measured traits, perhaps indicating an absence of trade-offs at least in the short term. Here we densely sample adaptive mutations in *Saccharomyces cerevisiae* to ask whether first-step adaptive mutations result in trade-offs during the growth cycle. We isolated thousands of adaptive clones evolved under carefully chosen conditions and quantified their performances in each part of the growth cycle. We too find that some first-step adaptive mutations can improve all traits to a modest extent. However, our dense sampling allowed us to identify trade-offs and establish the existence of Pareto fronts between fermentation and respiration, and between respiration and stationary phases. Moreover, we establish that no single mutation in the ancestral genome can circumvent the detected trade-offs. Finally, we sequenced hundreds of these adaptive clones, revealing new targets of adaptation and defining the genetic basis of the identified trade-offs.

That gain must ultimately be associated with some cost is a fundamental premise in fields spanning economics, engineering and biology. Biology in particular has a rich tradition of both alluding to and attempting to define trade-offs: here trade-offs imply that a part of trait space is not accessible by evolution such that, within a defined period of time, a lineage cannot evolve improved performance of two or more traits simultaneously above some threshold. Such evolutionary trade-offs have been suggested by various biological phenomena—for instance, organisms with high fecundity tend to have a short lifespan[1–3] and those with large eggs tend to lay fewer[4,5].

Despite the plethora of such examples of negative correlations between specific traits, such correlations alone are insufficient to demonstrate the existence of trade-offs. Indeed, many alternative explanations exist. For instance, consider an environment in which only one trait is under selection while a second is not. Over evolutionary time, performance in the first trait is likely to increase while performance in the second is likely to decrease due to the accumulation of damaging mutations in the absence of purifying selection[6,7]. At the same time, a reciprocal relationship may be observed in an alternative environment if the second trait is subject to selection and the first is not. This will lead to a negative correlation between performances of the two traits. However, it is entirely possible that mutations that improve both traits do exist but that they are not particularly common and not particularly advantageous in either of the environments. Additional explanations, such as sexual selection driving some traits to seemingly suboptimal states[8], or current selective pressures not corresponding to the way natural selection acted in the past, might also lead to negative correlations among traits in the absence of trade-offs. In short, negative correlation in performance between two traits is expected in the presence of trade-offs, but in and of itself is not sufficiently strong evidence for the existence of trade-offs.

Consider an organism with two traits under selection (Fig. 1a): its trait-fitness space is two-dimensional, with each axis representing performance for one of the traits. If a trade-off exists between the two traits, for every biologically possible value of trait 1, the best value for trait 2 performance will be constrained by trait 1, generating a Pareto optimality front (or Pareto front)[9]. Such a Pareto front not only represents the set of optimal trait combinations, but also separates the 'accessible' from the 'inaccessible' trait space. For individuals on the Pareto front (green dots in Fig. 1a), the existence of trade-offs can be demonstrated straightforwardly: increasing the performance for one trait will inevitably decrease that for another. By contrast, individuals behind the Pareto front (the black dot in Fig. 1a) are able to improve performance in both traits simultaneously. It is generally assumed that organisms should be located on or near a 'long-term' Pareto front, as they are products of very long-term evolution[1,2,5,9–12]. Surprisingly, results from experimental evolution often demonstrate the improvement of multiple traits simultaneously, suggesting that, at least for the conditions and traits tested, the ancestor does not lie on a Pareto front[13–19]. However, it is important to appreciate that it is possible for an individual to be on a higher-dimensional Pareto front, defined by multiple traits but, when measuring only a subset of the traits, the organism will appear to be behind the front (Fig. 1b). In this case, improvement in performance in the subset of traits must come at the cost of performance in the additional, unmeasured traits that contribute to the higher-dimensional front.

The Pareto front is typically thought of as being defined by physical, structural or physiological constraints and is usually considered to be static. However, the Pareto front may also be defined by genetic constraints, such that the space above the front might be locally inaccessible in the short term due to the rarity of specific genetic changes required to reach that region of trait space. For example, if the inaccessible part of trait space requires the system to move through a fitness valley, the system might remain at the Pareto front at least in the short term. The transition into the locally inaccessible part of the space would then be seen as a true evolutionary innovation that shifts the Pareto front to a new location.

[1]Departments of Biology, Stanford University, Stanford, CA, USA. [2]Departments of Genetics, Stanford University, Stanford, CA, USA.
*e-mail: dpetrov@stanford.edu; gsherloc@stanford.edu

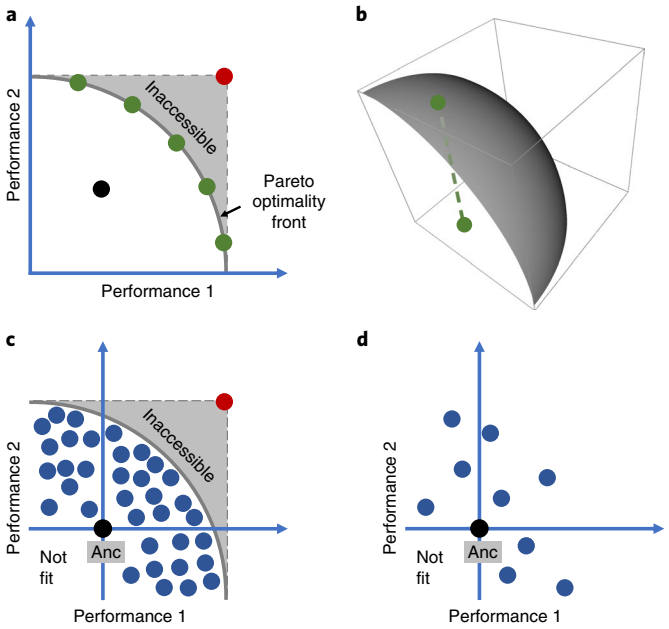

Fig. 1 | Evolutionary constraints in trait-performance space. **a**, The Pareto optimality front separates the evolutionary accessible space (white) from the inaccessible space (shaded). The red dot represents mutants that maximize both traits simultaneously. When organisms are on the Pareto optimality front (green dots), increasing the performance for one trait decreases that for the other. By contrast, when organisms are behind the Pareto front (black dot), organisms can improve the performance of both traits until the front is reached. **b**, An organism on a three-dimensional Pareto surface (green dot) appears to be suboptimal when it is projected onto a two-dimensional space. **c**,**d**, When the ancestor (Anc) is behind the Pareto front, many individuals occupying different parts of the trait space are required to characterize the Pareto front (**c**). By contrast, too few individuals are insufficient to delineate the front (**d**).

The Pareto front is thus defined by both the timescale of evolution and the physiological or structural relationships among the traits, and therefore may be dynamic over time.

To explore whether even the first step of adaptation can reveal evolutionary constraints in the form of Pareto fronts, one needs to sample a large number of adaptive mutants selected for multiple traits under a range of conditions, and then precisely measure their performance along each trait axis (Fig. 1c,d). Pareto fronts, if present, can then be inferred by an absence of mutants able to maximize both traits simultaneously (the large red dot in Fig. 1a,c). If the first-step mutations can reach the short-term Pareto optimality front and if the density of sampling is such that any adaptive single-step mutant that would land beyond the defined front would have been detected with high likelihood, then a short-term Pareto front will have been demonstrated.

Here we set out to investigate the existence of Pareto fronts among multiple traits, by evolving barcoded yeast populations under a number of carefully chosen conditions, selecting for improved performance in different phases of the yeast growth cycle, including fermentation, respiration and stationary phases. We isolated ~500 independent adaptive clones, most of which carry a single beneficial mutation. We found that a number of adaptive clones improved all three measured performances to a modest extent without apparent trade-offs, indicating that the ancestor cannot be located on a Pareto front for the measured traits. However, no adaptive clones were able to maximize performance in some pairs of traits. We were able to delineate apparent Pareto fronts between fermentation and respiration phase, as well as between respiration and stationary phase, but not between fermentation and stationary phase performance in our short-term evolution experiments. Importantly, due to a large number of sampled and tested clones we could assert that no single point mutation in the genome of the founding yeast strain in our experiment can improve the performance substantially beyond either of the two defined Pareto fronts. Finally, by sequencing hundreds of adaptive clones, we identified the genetic basis underlying the identified trade-offs and revealed new targets of adaptation.

Results

Experimental system and isolation of evolved clones. When yeast cells grow in conditions with a fermentable carbon source, such as glucose used in this study, they go through a sequence of growth phases: (1) lag phase, where cells acclimate to the medium, with no cell division; (2) fermentation, where cells divide exponentially by converting glucose into ethanol; (3) respiration, where glucose is exhausted and cells divide slowly by consuming the ethanol produced during fermentation; and (4) stationary/starvation phase, where cells cease growth because readily available carbon levels in the medium have been depleted (Fig. 2a).

To isolate adaptive clones with improved performance in fermentation, respiration and/or stationary phase (or combinations thereof), we propagated barcoded haploid yeast populations under four serial transfer conditions of differing cycle length: (1) 1-d (referred to as Evo1D), including 4-h lag, 16-h fermentation and 4-h respiration phases; (2) 2-d (Evo2D, conducted in ref. [20]) including additional 24-h respiration phase; (3) 5-d (Evo5D), including further 12-h respiration and 60-h stationary phases; and (4) alternating 1- and 5-d transfer (Evo1/5D) (Fig. 2a). Note that even though the same growth medium was used in the above conditions, we refer to them as different conditions because the differences in their transfer periods generate profoundly different selective pressures. We used barcode trajectories to determine whether cell cultures in cycle 11 contained a high proportion of diverse adaptive clones. Furthermore, our previous analysis indicated that at this time point most adaptive clones would contain only a single adaptive mutation[20]. Subsequent sequencing of individual clones (ref. [21] and see below) confirmed this supposition.

We isolated clones from cycle 11 for subsequent analysis. Specifically, from Evo1D, Evo2D, Evo5D and Evo1/5D we isolated, respectively, 120, 3,048 (isolated in ref. [21]), 157 and 384 distinct evolved clones carrying unique barcodes. We previously found that ~50% of clones isolated from Evo2D had self-diploidized during the course of evolution[21] and were beneficial across all fitness measurement conditions[22]. We therefore assayed the ploidy of newly isolated clones, and observed 43, 45 and 14% diploids among clones isolated from Evo1D, Evo5D and Evo1/5D, respectively.

We measured the fitness of all isolated clones in 1-d (Fit1D), 2-d (Fit2D), 3-d (Fit3D) and 5-d (Fit5D) serial transfer conditions (Fig. 2b; clones from Evo2D were measured in ref. [22]) using the method developed in ref. [21]. For each clone, we therefore have its fitness in both the 'home' condition (except for Evo1/5D clones) and the 'away' condition. Note that one condition (Fit3D) was not used as an evolutionary condition but instead was important for evaluation of stationary phase performance. Below we use these values to investigate patterns of local adaptation and to estimate the performance of each clone in the fermentation, respiration and stationary phases. Using the fitness and ploidy measurements, we identified 66, 144, 58 and 132 adaptive haploids and four, 40, 57 and six high-fitness diploids (assumed to have additional beneficial mutations besides diploidy) from Evo1D, Evo2D, Evo5D and Evo1/5D, respectively. We refer to these adaptive haploids and high-fitness diploids collectively as adaptive clones.

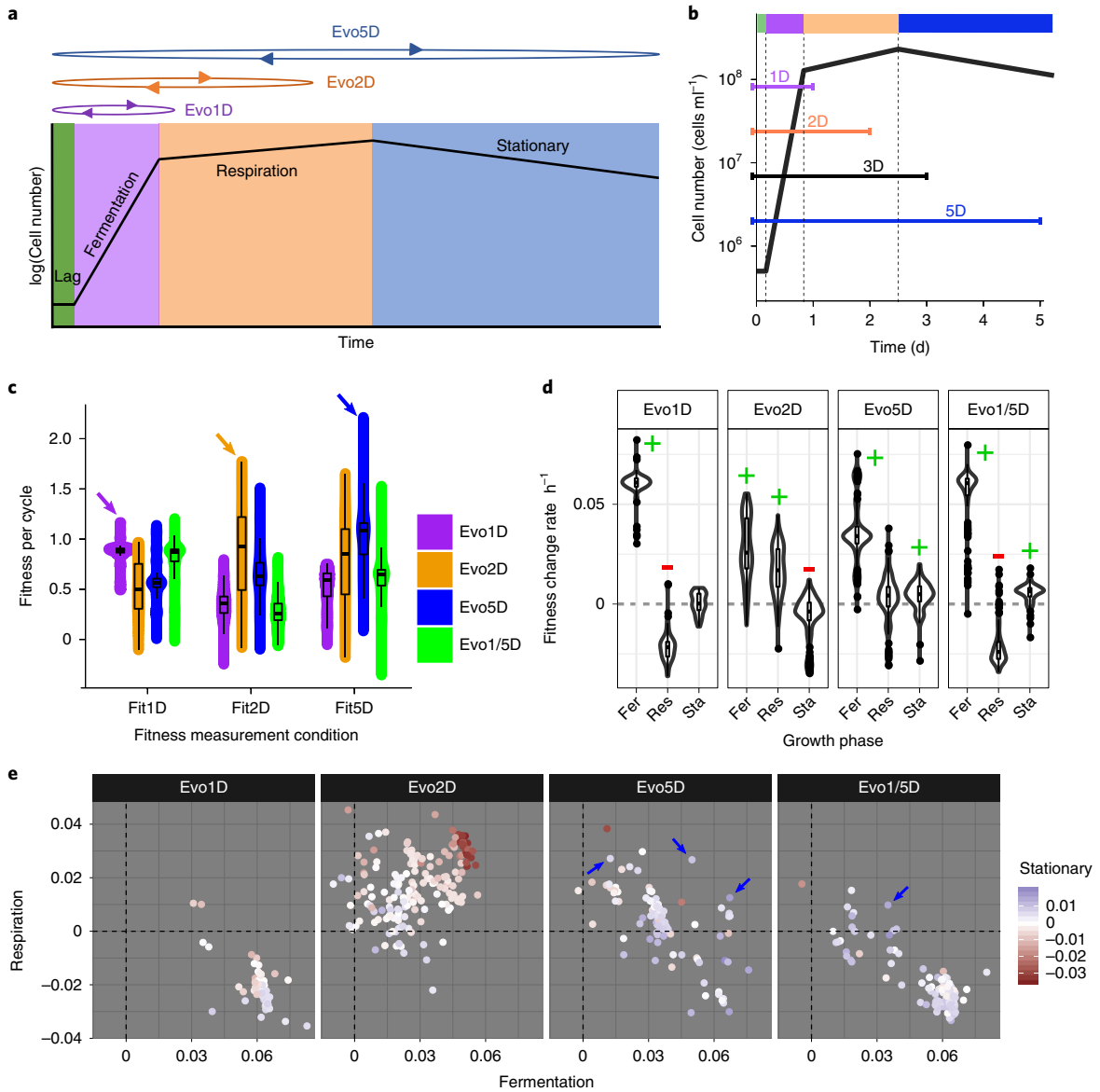

Fig. 2 | Experimental design and observation of local adaptation and trade-offs. a, Three chosen evolutionary conditions span different phases of the yeast growth cycle. Clones were also evolved in Evo1/5D. **b**, Fitness measurement conditions designed to quantify fermentation, respiration and stationary performance (fitness change h^{-1}) of each clone. Dashed vertical lines separate different growth phases, coloured as in **a**. **c**, Fitness measurements of adaptive clones, grouped by their home evolutionary condition, in home and away conditions. Arrows indicate adaptive clones measured in their home condition. The lower and upper hinges of each box correspond to the first and third quartiles (25th and 75th percentiles). The whiskers extend from the hinge to a value no further than 1.5× interquartile range from the hinge. The width of the violin represents the probability density of the data at different fitness values. **d**, Performance of adaptive clones' fermentation (Fer), respiration (Res) and stationary (Sta) phases grouped by their evolutionary condition. + or − indicate increased or decreased performance, respectively, compared with the ancestor. **e**, Clones are separated by their evolutionary condition and coloured by their stationary phase performance. Each dot represents a clone. Note that some blue-coloured clones from Evo5D and Evo1/5D (indicated by arrows) improve performance in all three growth phases.

Local adaptation results from performance differences in different growth phases. We observed a wide range of fitness in both the home and away environments (Fig. 2c). For example, the fitness of all adaptive clones varied from −0.35 to +2.2 per growth cycle in Fit5D, suggesting multiple adaptive strategies and targets of adaptation among these clones. While only 4.5% of the adaptive clones are maladaptive in any away condition, we find that, in general, adaptive clones exhibit evidence of local adaptation. Specifically, for each fitness re-measurement condition, both the average and highest fitness of clones evolved in the home condition (indicated by arrows) are greater than those of clones evolved in the away conditions. Nonetheless, under a given fitness measurement condition, not all 'home' clones are more fit than all 'away' clones.

We further used our combined fitness data to determine the performance of individual clones in three of the phases in the growth cycle: fermentation, respiration and stationary (Fig. 2d). Here, as cells spend different amounts of time in each growth phase, we define performance as the increase in fitness, per hour, for a given growth phase; our previous study demonstrated that the overall fitness scales linearly with the amount of time spent in each of the growth phases[22]. The slope of the relationship between the relative fitness of a clone and the length of a particular growth phase

Table 1 | Genetic basis of adaptation and trade-offs

		Evo1D	Evo2D	Evo5D	Evo1/5D
RAS/PKA	*CYR1*	0	3	1	1
	GPB2	0	13	0	0
	RAS2	0	2	0	0
	IRA1	0	39	0	0
	IRA2	0	10	1	0
	PDE2	0	11	0	0
TOR/Sch9	*TOR1*	0	1	0	0
	SCH9	0	1	0	0
	SXM1	12	1	10	26
	CHR11 DUP	0	4 (diploid)	11	1
	FPK1	0	1	10	2
HOG	*SSK1*	0	0	7	0
	SSK2	0	2	1	0
	HOG1	0	0	1	0

The number of clones carrying recurrent mutations within genes or pathways. These genes/pathways were independently mutated more than four times. Genes in the same pathway are grouped by the large parenthesis on the left.

(measured as fitness change per hour) can thus be used as a measure of clone performance in that phase. For instance, as the clones spend an extra 24 h in respiration during every cycle when growing under Fit2D compared to Fit1D, we can calculate respiration performance by subtracting the relative fitness of each clone in Fit1D from that in Fit2D and then dividing by 24 h: (Fit2D – Fit1D)/24. Similarly, we calculated the fermentation ((Fit1D – 4 × respiration performance)/16, as cells go through 4-h respiration and 16-h fermentation in the 1-d condition) and stationary performances ((Fit5D – Fit3D)/48) (Methods, 'Quantification of performance in growth phases').

We compared these three performances for clones evolved in all four conditions. Overall, while clones from each condition often revealed specific and consistent patterns of apparent trade-offs, the trade-offs observed were not necessarily shared across all conditions (Fig. 2d,e). For example, we previously found that most adaptive clones from Evo2D have improved performance in both fermentation and respiration, but decreased performance in stationary phase[22]. By contrast, adaptive clones from Evo1D have improved performance in fermentation yet decreased performance in respiration and nearly unchanged performance in stationary phase. Most adaptive clones from Evo5D exhibit yet another different pattern—improved performance in both fermentation and stationary phases—but their performance in respiration on average is largely unchanged. Finally, adaptive clones from Evo1/5D have improved fermentation and stationary phase performance and generally decreased respiration performance. Overall, we found adaptive clones that improved every pair of fermentation, respiration and stationary phase performance, as well as some that showed improved performance across all three (indicated by arrows in Fig. 2e), suggesting that the ancestor is behind any potential Pareto front for these three performances.

The genetic basis of adaptation and trade-offs. We determined the genetic basis of adaptation by genome-wide sequencing of 47, 67 and 85 adaptive clones from Evo1D, Evo5D and Evo1/5D, respectively. Putative adaptive mutations were successfully identified in 35 (74%), 66 (98%) and 81 (95%) of these clones, respectively. The identity of 125 adaptive mutants from Evo2D was determined previously[21,22]. Many genes or pathways were recurrently mutated in our adaptive clones—in such cases we can be confident that these mutations are indeed adaptive. Specifically, out of the 182 adaptive clones in which we identified putative adaptive mutations, 118 (~65%) harbour mutations in genes/pathways hit in multiple clones (Supplementary Table 3). Furthermore, 79 of these harbour mutations in genes/pathways independently hit five or more times (Table 1).

In general, within each evolutionary condition, beneficial mutations were limited to a small number of genes that serve similar biological functions. At the same time, across evolutionary conditions, beneficial mutations tend to differ in their genetic bases (Table 1). For instance, we previously reported that the majority of adaptive mutants for Evo2D upregulated the RAS/PKA and TOR/Sch9 nutrient-sensing pathways[21], but we rarely recovered adaptive mutations in these pathways from other evolutionary conditions. By contrast, loss of function in *SXM1* (also known as *KAP108*, which encodes a ß-karyopherin[23,24]) was the prevalent cause of adaptation in Evo1D. Karyopherins mediate transport through the nuclear pore. Sxm1 functions as an importin and, in an *sxm1*Δ strain, the localization of Tpk2 (one of the catalytic subunits of protein kinase A (PKA)) to

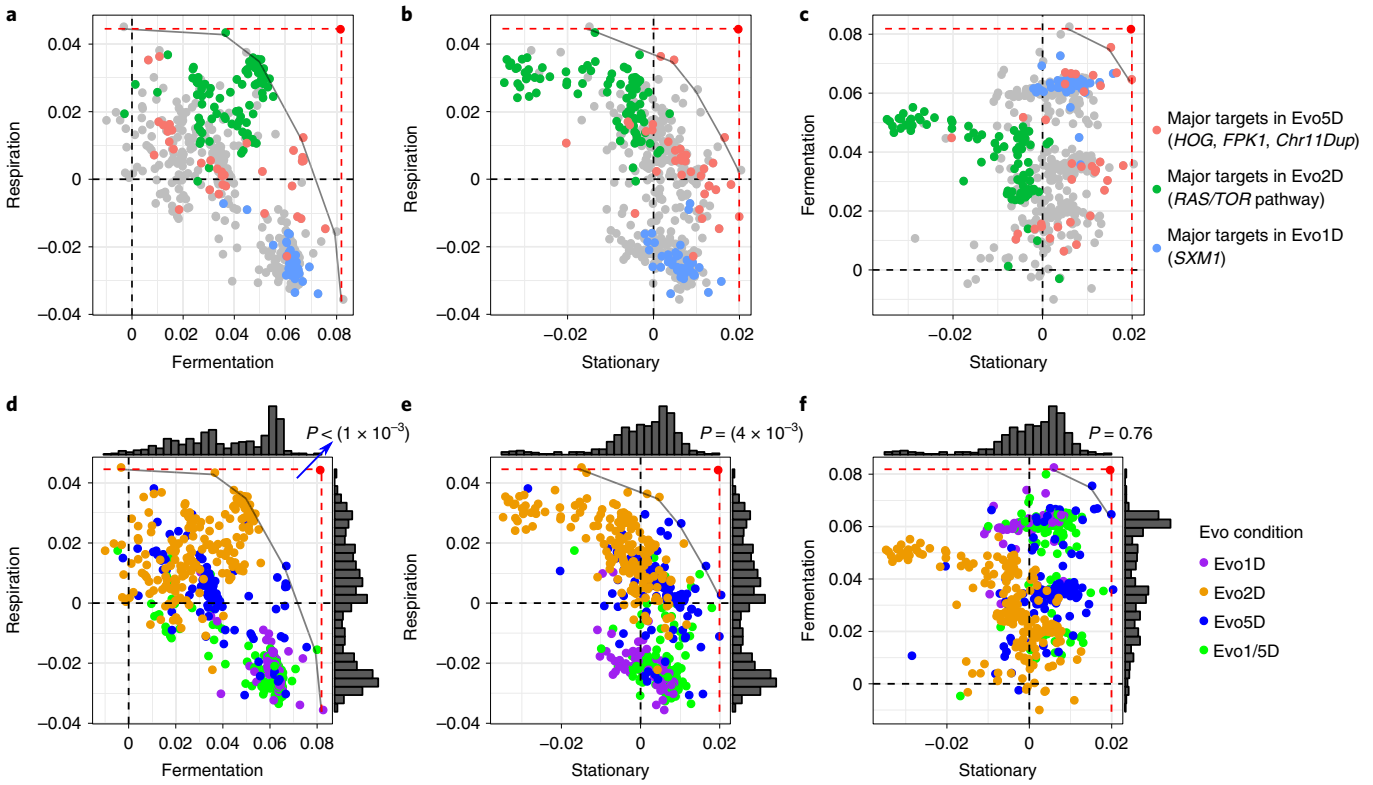

Fig. 3 | Mapping of the evolutionarily accessible trait space. a–f, For each pair of performances (fitness change h^{-1} in each growth phase), adaptive clones are plotted and coloured according to either their molecular basis (**a–c**) or their evolutionary conditions (**d–f**). Each dot represents a clone. The large red dots represent the optimum phenotypes, achieving the upper limits (dashed lines) of each pair of performances. The grey curves, defined by the convex hull algorithm, represent putative Pareto optimality fronts. **d–f**, Histograms to the side represent the density distribution of each trait's performance. Based on the null distribution, the *P* value of observing an empty space between the putative front and the optimal type (large red dot, top right) as large as that observed in the real data is reported.

the nucleus in response to stress is abrogated[25], and its chromatin association is abolished. Thus, in an adaptive strain from Evo1D carrying a loss-of-function mutation in *SXM1* it is possible that Ras/PKA activity is diminished, potentially explaining the loss of fitness in respiration experienced by these mutants. While *SXM1* mutants were also observed in Evo5D, they were not the predominant mutant class. Rather, a wide variety of mutations were observed among Evo5D adaptive clones, including (1) 11 duplications of chromosome 11 (*Chr11Dup*), (2) ten independent loss-of-function mutations in *FPK1* and (3) nine mutations in three components of the high-osmolarity glycerol (HOG) response pathway: *SSK1*, *SSK2* and *HOG1*. Given that Evo5D includes a long period of starvation, observation of *Chr11* aneuploidy is consistent with previous findings that aneuploidies can improve survival under extremely stressful conditions[26–28], although the underlying mechanism is unknown. *FPK1* (a flippase activator) has previously been shown to increase viability in stationary phase[29], which we experimentally confirmed (Supplementary Table 4). The genetic bases of adaptation among Evo1/5D clones were similar to those for Evo5D clones, with mutations in *SXM1* and *FPK1* as well as duplication of *Chr11*.

Next, we examined the relationship between the identified genetic basis of adaptation and the resulting increases/decreases in performance (Fig. 3a–c). As stated above, in this study 'performance' represents fitness change per hour in a particular growth phase rather than measurement of physiological traits (for example, growth rate) as it is commonly used. Due to population dynamics, the genetic outcome of each evolutionary condition is biased towards the observation of mutations in genes with a large target size and high fitness. Even though we have sampled a large number of clones from multiple conditions, mutations that arise too infrequently or are insufficiently adaptive do not end up contributing to adaptation in the culture and thus are not sampled. For instance, the *SXM1* mutants, predominant in Evo1D, have among the highest observed fermentation performance, at >6% h^{-1} (giving >96% fitness advantage over the ancestor over the full 16-h period of fermentation under our conditions). This probably explains why nutrient-sensing RAS/PKA and TOR/Sch9 pathway mutants, which have lower fermentation performance than the *SXM1* mutants, were not observed in Evo1D. However, the high fermentation performances of *SXM1* mutants come at a cost of reduced respiration performance (−2–3% h^{-1}). This probably explains their near absence in Evo2D, given that the Evo2D condition contains a long period of respiration. This allows the RAS/PKA and TOR/Sch9 mutants to dominate Evo2D conditions. Similarly, the most prevalent Evo2D RAS/PKA nutrient-sensing pathway mutants with the highest respiration performance trade off strongly in stationary phase[22], explaining why they were not observed in Evo5D. Finally, clones that are common in Evo5D, which contains all phases of the growth cycle, are the least likely to show decreased performance in any phases of the growth cycle. Indeed, Evo5D-specific mutations, such as *Chr11* duplication and *SSK1* mutation, show no obvious trade-offs but rather modest improvements in one or more performances (Supplementary Fig. 1). Interestingly, Evo5D clones also include *SXM1* mutants that show increased performance only in fermentation, with decreased performance in respiration and little change in stationary phase. In this case, their strong improvement in fermentation and lack of trade-off in stationary phase appear to compensate adequately for their reduced fitness in respiration.

In summary, adaptation under these conditions is idiosyncratic yet predictable: the genetic basis of adaptation under a particular evolutionary condition tends to target a narrow, recurrent and thus a posteriori predictable set of genes. However, these gene targets are not shared across all environments, meaning that adaptation across conditions often relies on entirely different genetic pathways. This idiosyncratic nature explains the specific patterns of performance across conditions (Fig. 2d,e). While we detect clones that increase all performances, those that perform best in any one growth phase tend to trade off in performance in some other growth phase(s). This hints at the existence of evolutionary constraints preventing the emergence of adaptive clones that simultaneously maximize performance in all growth phases.

Identification of evolutionary constraints and delineation of Pareto fronts. We observed an absence of clones near the upper limits of either both fermentation and respiration performance, or both respiration and stationary performance (the large red dot in Fig. 3a,b,d,e). Thus, there is at least the appearance of an empty space in the upper right corner where these pairs of performances would be maximized. We used the convex hull algorithm to delineate potential Pareto fronts that separate the short-term, evolutionarily accessible space from the empty, putatively short-term inaccessible space above the front (grey curves in Fig. 3).

We first tested whether, given the marginal distributions of trait performance, the size of the empty space at the top right of those plots is surprisingly large (Methods). Under a null hypothesis of independence of performance, the observation of such large empty spaces is indeed unexpected ($P<1\times10^{-3}$ for fermentation and respiration phases and $P=4\times10^{-3}$ for respiration and stationary phases; Fig. 3d,e and Supplementary Fig. 2). By contrast, the size of the empty space between fermentation and stationary performance is not unexpected (Fig. 3f and Supplementary Fig. 2; $P=0.76$).

The mutational target size of the optimal types is smaller than a single nucleotide. To further explore the absence of clones beyond the putative Pareto fronts, we determined the target size for potential single-step mutations that would give rise to maximum performance for fermentation and respiration, or respiration and stationary phases (marked by the large red dot in Fig. 3a,b,d,e). Mutants that could maximize two traits simultaneously would be more fit than the observed mutants, at least under certain evolutionary conditions; thus, based on this increased fitness, such mutants, should they arise at a rate similar to that of the observed mutants, should be sampled frequently under those conditions. For example, mutants that improve fermentation and respiration simultaneously beyond the putative front should have a higher fitness than most of the sampled clones in Evo2D (Supplementary Fig. 3), as clones in this condition experience only fermentation and respiration. Likewise, clones that improve respiration and stationary phases beyond the putative front should have a high fitness in Evo5D (Supplementary Fig. 3), given that the majority of clones with high respiration or stationary performance also have a positive fermentation performance. The fact that we did not observe any clones beyond the putative fronts suggests that the genomic mutational target size towards such extremely fit mutants located beyond the putative Pareto fronts must be smaller than that for the observed mutants. Furthermore, we demonstrated that our evolution experiments were not mutation limited. Indeed, given the observed mutation rate of $\sim3\times10^{-10}$ per base pair (bp) per generation (1 bp is mutated into a specific nucleotide, A, T, C or G), the effective population size of $\sim6\times10^{8}$ and the number of generations before sampling (~80), each base pair is expected to have been mutated into one specific nucleotide ~15 times by the time of our sampling.

Next, we used a mathematical model to quantitatively assess the probability of sampling a single-step mutation with a given selection coefficient, s (Methods). Several factors determine the probability of sampling such a single-step mutation: (1) the rate at which a mutation occurs, (2) the probability of such a mutation surviving random drift and establishing in the population (approximately proportional to s) and (3) the exponential division rate after the mutation establishes (its cell number reaches roughly e^{st}, with t generations between establishment and sampling). With mutations entering the population at a fixed rate, the more fit a mutant is (the larger s is), the more likely that mutant establishes in the population, the faster it divides and eventually the higher the frequency the mutant reaches by sampling time.

First, consider a gene with the same target size for adaptive mutations as *IRA1* (mutations in which were observed 39 times after sampling at cycle 11 of Evo2D[21,22]), but whose mutation results in a fitness benefit at the hypothetical optimal type with maximal fermentation and respiration (the red dot in Fig. 3a,d). Such a hypothetical mutant would have a fitness of ~2.56 per cycle in Evo2D, compared to ~1.64 per cycle for *IRA1*-nonsense mutations. If such a hypothetical gene exists, we would expect to observe mutations in this gene ~25,000 times more frequently than we observed mutations in *IRA1* in Evo2D ($e^{(2.56\times11)}/e^{(1.64\times11)}$). Thus, it is exceptionally unlikely that such a gene with a target size similar to that of *IRA1* does exist. Furthermore, if the target size for such a gene is just a single base pair, our mathematical model suggests that we would expect to see such a mutation between 84 and 99% of the time in our evolution experiments (Methods). Thus, we believe it is unlikely that there is even a single site in the genome of the ancestral strain that can be mutated to provide such a high fitness.

Similarly, the hypothetical optimal type that maximizes respiration and stationary phase performance would have a fitness benefit of ~2.98 per cycle in Evo5D (represented by the red dot in Fig. 3b,e) (assuming a fermentation performance of zero). If a single site (1 bp) can be mutated to this hypothetical optimal type, we would expect to sample such a mutant between 88 and 98% of the time in Evo5D experiments. Thus, there is probably no single-step mutation in the ancestral yeast genome that can simultaneously maximize the performance of both fermentation and respiration, or both respiration and stationary, to its highest observed level.

Discussion

Despite the fact that trade-offs have been widely assumed in studies of evolution, it is extremely challenging to formally establish their existence. Here, by sampling a large number of adaptive clones from a range of evolutionary conditions and measuring their performance in three different growth phases, we were able to demonstrate the existence of Pareto fronts between performance in the fermentation and respiration phases, and between the performance in the respiration and stationary phases. Furthermore, we were able to show that the ancestor must be behind these fronts because, for both pairs of traits, there were clones that were able to improve performance in both traits simultaneously; indeed, some clones were able to improve performance in all three growth phases.

A large number of diversely selected adaptive clones is needed to delineate Pareto fronts. If the ancestor was on a front delineated by two traits, characterization of that front using experimental evolution would be straightforward because no adaptive clones could improve both traits simultaneously—indeed, by definition, improvement of performance in one trait would lead to a loss of performance in the other. However, because the ancestor lies behind the fronts we identified, only by mapping a very large number of adaptive clones whose performance spans the trait space could we map the Pareto fronts. By randomly subsampling our data, we estimated that between roughly100 and 300 independent adaptive mutants are required to detect the Pareto fronts in our experiment (Methods). Furthermore, given that clones isolated from a particular

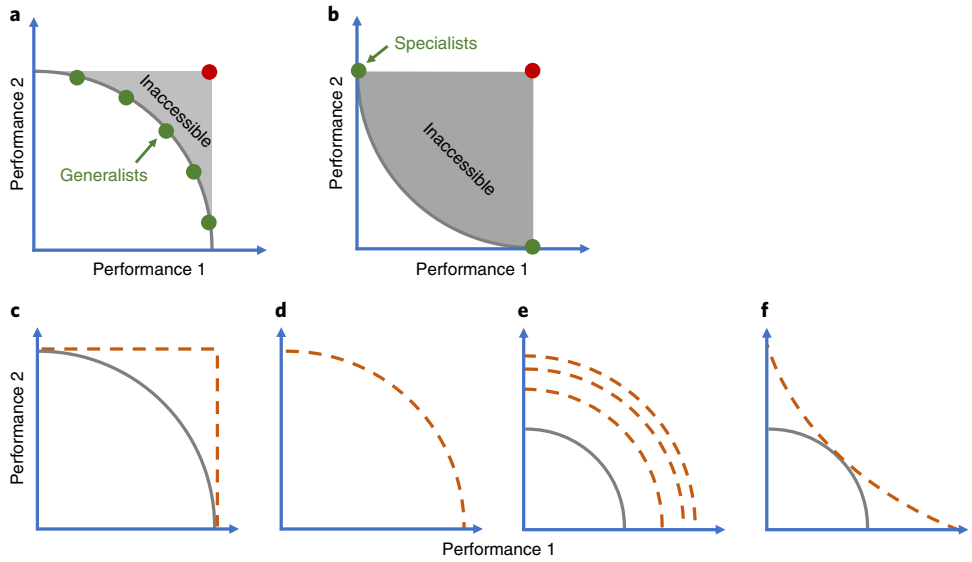

Fig. 4 | Pareto front geometry and potential changes over longer-term evolution. a,**b**, During evolution, the convex-shaped Pareto front (**a**) favours generalists, while the concave-shaped front (**b**) favours specialists. **c**–**f**, The current convex Pareto front (solid grey curve) can change into a rectangle (**c**), with the previously inaccessible space being populated, stay in place (**d**), move forward while keeping its shape (**e**) or change its shape over longer-term evolution (**f**). Potential Pareto fronts following longer-term evolution are depicted by orange dashed lines.

evolutionary condition—for example, Evo1D—tend to occupy a specific part of the trait space, clones from Evo1D, Evo2D and Evo5D together were required to detect the Pareto fronts.

Finally, having such a large number of adaptive clones enabled us to show that, for both of the identified Pareto fronts, there is no single mutation that can occur in the genome of the ancestral strain that would enable that strain to maximize performance in both traits. These fronts therefore constrain the evolutionarily accessible space over short timescales.

No Pareto front observed between fermentation and stationary phases. We were unable to identify a Pareto front between fermentation and stationary phase performance, suggesting either an absence of trade-offs between these two traits or that single-step mutations provide insufficient performance improvement to reach a hypothetical Pareto front. However, this may also be due to experimental limitations—specifically, clones selected under Evo5D experienced both fermentation and respiration before stationary phase. Thus, it is entirely possible that the maximum stationary phase performance is higher than we observed, if clones with such a large stationary phase performance trade off strongly in fermentation or respiration. A longer stationary phase—for example, a 10-d serial transfer—may help select for such mutants and define a Pareto front between fermentation and stationary phase performance should one exist. Additionally, evolution in a non-fermentable carbon source, followed by a long stationary phase, may also enable selection of clones with high stationary phase performance that trade off strongly in fermentation.

The shape of Pareto fronts and nature of trade-offs. It was suggested that the geometry of Pareto fronts will affect an organism's evolvability, and whether generalists or specialists will tend to evolve[30]. For instance, a convex-shaped front allows for better evolvability and produces different optimal types based on the particular evolutionary condition, allowing for local adaptation (Fig. 4a). By contrast, a concave-shaped front leads to less evolvability because, regardless of the importance of performance in each trait, one of the two most specialized types will always be the most fit (Fig. 4b).

Previous studies have used, for example, ecological data in phytoplankton[31], interactions between phage and *Escherichia coli*[32] and synthetic, *E. coli*-based systems[33] to investigate the geometry of Pareto fronts and, in one case, it has been shown that an evolving ancestor is probably on a Pareto front[12]. However, no study has yet quantitatively defined a Pareto front or characterized its geometry in evolving populations where the ancestor lies behind the front, which is the case in most experimental evolutions. Here we identified not one, but two, convex-shaped fronts for two independent trade-offs under well-controlled selection pressures in our short-term evolution experiments. There are two important points to consider. First, we note that despite evolving under different transfer regimes that subjected cells to distinct selective pressures, each regime used the same growth medium with a defined glucose concentration. It will be important to determine whether even subtle variations in this growth medium would change the selective pressures and, in doing so, would alter or even eliminate the observed Pareto fronts. Second, it is possible that the shape of the Pareto front itself may change over the timescales of evolution[34,35], and the way in which it might change will be informative about whether the observed front is due solely to a genetic constraint or, instead, whether there is an underlying intrinsic physiological constraint.

Over longer-term evolution, the space that is inaccessible in the short term may become populated and the shape change becomes a rectangle (Fig. 4c). This would imply that there is no physiological constraint between the two traits and that the observed Pareto front is purely due to a genetic constraint—that is, no clones with single mutations are able to occupy the seemingly inaccessible space, yet those with multiple mutation can. Alternatively, the front may either stay in place (Fig. 4d) or move forward but retain the same shape (Fig. 4e), always defining an inaccessible space. This scenario would suggest intrinsic physiological constraints whereby no single individual could maximize performance in both traits simultaneously. A final possibility is that longer-term evolution may change the shape of the front from convex to concave (Fig. 4f), such that individuals with extreme performance in one or the other trait are the most fit depending upon the exact condition in which they are evolved.

The behaviour of clones containing multiple adaptive mutations should provide some insights. We observed three clones carrying

two adaptive mutations, each in genes specific to different evolutionary conditions. These clones harbour mutations in *SXM1* and *HOG1*, *SXM1* and *SSK1*, and *SXM1* and *CYR1*, respectively. We observed that each of these double mutants is no closer to the front than the corresponding single mutants (Supplementary Fig. 4), suggesting the front itself might be moderately stable. However, clearly both long-term and further evolution of already adaptive clones under various conditions are needed to test this.

Future prospects. Despite much focus on the study of trade-offs in ecology and evolution, rigorous demonstration of trade-offs has proved surprisingly difficult[15,36]. Furthermore, even when trade-offs have been demonstrated, the underlying causes typically remain elusive—the genetic bases of adaptation and trade-offs identified here provide additional potential targets for further investigation of whether the detected trade-offs are caused by intrinsic physiological constraints. Here we have shown that it is possible to use barcoding and experimental evolution across a range of conditions to isolate a sufficiently large number of adaptive mutants that, together, can map the shape of the evolutionary accessible trait space in short-term evolution, from which trade-offs can be inferred. Our approach is generic and can be used to study trade-offs between multiple traits, including ecologically relevant traits such as the ability to sporulate or undergo mating, and can be performed with different founding strains and species. Such studies hold promise in helping us to understand the shape of trade-offs among multiple traits, in both pairs and higher dimensions.

Methods

Founding populations and experimental evolution. *Barcoded yeast populations.* Barcoded yeast populations were constructed as in ref. [20]. However, whereas those workers used only one landing-pad yeast strain (SHA185), we used multiple landing-pad yeast strains with each strain carrying a unique, condition-specific barcode. Next, a high-complexity plasmid library was introduced into each landing-pad strain through transformation; correct integrants were selected for uracil prototrophy[20]. These transformants contain both a low-complexity, condition-specific barcode and a high-complexity, lineage-tracking barcode. Three barcoded yeast populations with distinct condition-specific barcodes were constructed. Each barcoded yeast population includes around half a million unique transformants. These three barcoded yeast populations were evolved under Evo1D, Evo5D and Evo1/5D, respectively.

Yeast growth media and growth cycle. All cultures were grown in 100 ml of M3 medium[20] (5× Delft medium with 4% ammonium sulfate and 1.5% dextrose) in 500-ml Delong flasks (Bellco) at 30 °C and 223 r.p.m. This culture condition is referred to as our standard culture condition.

Yeast cells go through different growth phases when growing under a glucose-limited condition—lag, fermentation, respiration and stationary. Based on our previous study[22], with 5×10^7 cells inoculated into our standard culture condition, cells experience lag phase for ~4 h, fermentation for ~16 h, respiration for ~40 h and stationary phase thereafter[22]. Wild-type cultures reach a saturation cell number ~1.7×10^8 ml^{-1}, and thus the final population size is ~1.7×10^{10}. We note that these parameters can change somewhat under different growth conditions. For example, cells experience a longer lag phase under Evo5D because they entered stationary phase in the previous growth cycle. Such variations are not taken into account in our analyses. Furthermore, these parameters are variable across different genotypes. For instance, the tested *IRA1-nonsense* mutation saturated around 1.1×10^8 ml^{-1} after 2-d growth[22].

Serial batch transfer during evolution. The barcoded yeast populations were evolved by serial batch culture in M3 medium. Under Evo1D, bottlenecks were performed by the addition of 7×10^7 cells of the culture from the previous growth cycle to fresh media; cells were grown for 24 h between each bottleneck. Cells were highly viable (close to 100%) after 1 d of growth. Cell counts were performed at each bottleneck to estimate the generation time. Cultures reached ~9×10^7 cells ml^{-1}, with a final population size ~9×10^9. Thus, cells went through approximately seven generations during each transfer in Evo1D ($\log_2(9\times10^9/7\times10^7)=7$ generations). Populations were evolved for up to 25 growth cycles (~175 generations).

Under Evo5D, bottlenecks were performed every 5 d. Cultures reached ~1.25×10^8 cells ml^{-1}, with a final population size ~1.25×10^{10}. Cell viability decreased during the stationary phase. To avoid strong bottleneck drift, cell viability was estimated at each bottleneck and 7×10^7 viable cells were inoculated into the next serial transfer. Viability was estimated by counting colony-forming units on yeast peptone dextrose (YPD) plates and then dividing their number by that of the cells plated. Cells went through ~7.5 generations during each transfer in Evo5D. Cells were evolved up to 16 cycles (~120 generations).

Under Evo1/5D, cells were bottlenecked every 1 and 5 d, alternating; 7×10^7 viable cells were inoculated at each bottleneck. Similarly, cells went through roughly seven generations during 1-d transfer and roughly 7.5 generations during 5-d transfer. Cells were evolved up to 23 cycles by alternating between 1- and 5-d transfers (~166 generations).

Two replicates were conducted under each evolutionary condition. At the end of each transfer, 2 ml cell culture of evolution was mixed with 1 ml 40% glycerol, aliquoted into two Eppendorf tubes and stored at −80 °C. The remainder of the cell culture (>95 ml, besides a small amount used to inoculate the next cycle) was centrifuged, then the cell pellet was resuspended in 5 ml sorbitol solution (0.9 M sorbitol, 0.1 M Tris-HCL pH 7.5, 0.1 M EDTA pH 8.0), aliquoted into 2-ml Eppendorf tubes and stored at −20 °C for genomic extraction.

In addition, Evo2D evolution was conducted as in ref. [20], where bottleneck was performed by the addition of 400 µl (~5×10^7 cells) to fresh media. Cells went through around eight generations per cycle.

Tracking lineage dynamics during evolution. *Library preparation and sequencing.* To track changes in lineage frequency over the course of evolution, cells collected at the end of every three transfers under Evo1D, Evo5D and Evo1/5D were used for genomic DNA extraction. Genome extraction and PCR amplification of the barcode region were conducted as in ref. [21]. Amplicons were sequenced on Illumina HiSeq 4000 (2×101 paired-end). Data for Evo2D can be found in ref. [20]. A perfect sequencing read should follow this DNA sequence: NNNNNNNNXXXXXTT-AATATGGACTAAAGGAGGCTTTTGTCGACGGATCCGATATCGGTACC (+26-bp lineage barcode+) ATAACTTCGTATAATGTATGCTATACGAAGTTAT (+26-bp condition barcode+) GGTACCGATATCAGATCTAAGCTTGAATTCGA TXXXXXXXXXNNNNNNNN.

The Ns in the sequence are random nucleotides, and are used as unique molecular identifiers (UMIs) in the downstream analysis to remove skew in the counts caused by PCR jack-potting[20]. The Xs correspond to multiplexing tags, which allow distinguishing between different samples when loaded on the same sequencing flow cell[20].

Barcode counts. Sequencing reads, with 17 bp (including the UMIs and multiplexing tags) on both the 5′ and 3′ ends removed, were first aligned to the reference barcode region using Bowtie2. Based on this alignment, both condition and lineage barcodes were extracted. Next, the UMIs, multiplexing tags and barcodes were re-associated for each pair of reads. Reads were split into different files based on their multiplexing tags, representing the sample from which the reads came. Last, reads from the same sample were clustered using Bartender[37] with Hamming distance 2 and seed length 8. The final output includes both barcode sequences and counts of each lineage. Each lineage is represented by a unique combination of condition and lineage barcodes. Reads with the same combination of UMI, multiplexing tags and barcodes were counted as one read because they were probably caused by PCR jack-potting. An extra round of clustering was conducted using barcode combinations identified by Bartender to further cluster barcodes with ≤2 Hamming distance. On average, each sample has ~1.3 million high-quality reads. For each evolution replicate, lineages with fewer than ten counts across all time points and lineages present at fewer than three sequenced time points were filtered out. Barcode counts over the course of evolution can be found in Supplementary Table 1.

Isolation of clones from evolution. *Isolation of evolved clones from evolutionary conditions.* Based on population dynamics, yeast clones were isolated from frozen samples of Evo1D, Evo5D and Evo1/5D at cycle 11. Frozen stock (~50 µl,containing ~3.5×10^6 cells) was diluted into 500 µl PBS plus 1 µl propidium iodide and used for flow cytometry sorting. Single cells were sorted into 96-well plates with 100 µl YPD medium in each well. Sixteen plates of cells (~1,500 cells) were sorted for each evolutionary condition with eight plates from each replicate (48 plates in total, sorted from Evo1D, Evo5D and Evo1/5D). Sorted cells were grown at 30 °C for 3 d without shaking, and reached saturation by day 3. Saturated cell culture (~5 µl) was removed from each well and inoculated into a different 96-well plate, with 100 µl fresh YPD medium in each well. These replicated plates were grown at 30 °C for 2 d without shaking to reach saturation, and used for subsequent ploidy and barcode identification. The remainder of the saturated cell culture was mixed with 100 µl 50% glycerol and stored at −80 °C.

Ploidy test. A high-throughput ploidy test was developed using the drug benomyl[21]. Saturated cultures from the 48 replicated 96-well plates were mixed and pinned onto YPD + 20 µg ml^{-1} benomyl (in DMSO) on rectangular agar plates using a multi-pronged pinner, grown at 25 °C for 48 h and then imaged. Under these conditions, diploid growth was strongly inhibited by benomyl but haploid growth was less affected.

DNA barcode identification by Metagrid. Saturated cell culture (20 µl) was removed from each well of the replicated plates into 96-well PCR plates. Cells were lysed by

incubation at 95 °C for 15 min. Lysed cell culture (5 µl) was used to PCR amplify the DNA barcode region. To reduce the cost of Sanger sequencing to ~4,600 clones, a Metagrid approach was developed. Seventy-two forward and 64 reverse primers were synthesized, with each primer carrying an 8-bp unique multiplexing tag (Ns in the primer sequence). Each PCR well was coded by a unique combination of forward and reverse multiplexing tags. Two-step PCR amplification was conducted here, with the first step using multiplexed primers and the second using standard Illumina paired-end ligation primers (PE1 and PE2). PCR products from all 48 plates were pooled and sequenced using Illumina NextSeq (2 × 150 paired-ends):

- forward primer of first-step PCR: ACACTCTTTCCCTACAC-GACGCTCTTCCGATCTNNNNNNNNTTAATATGGACTAAAGGAG-GCTTTT
- reverse primer of first-step PCR: CTCGGCATTCCTGCTGAACCGCTCTTC-CGATCTNNNNNNNNTCGAATTCAAGCTTAGATCTGATA

Regular expressions that match DNA sequences flanking multiplexing tags of primer and clone barcodes were used to extract multiplexing tags and barcodes. A map between clone DNA barcodes and their physical position on the 96-well plates was constructed based on multiplexing tags. The number of clones carrying unique barcodes is lower than that of clones isolated, due to the lack of growth in a small number of wells and, more importantly, to the high frequency of a few adaptive clones—a large number of isolated clones carrying the same barcodes; 124, 166 and 397 unique barcodes were identified from Evo1D, Evo5D and Evo1/5D, respectively.

High-throughput fitness measurements. *Pool of clones for fitness measurements.* Isolated clones with a unique barcode were pooled for high-throughput fitness assay. Note that some barcodes were present in both haploid and diploid clones—for those barcodes, only the former were pooled for fitness assay. Clones with a unique barcode were hand-picked from previously frozen stock and re-arrayed onto a set of 96-deep-well plates with 700 µl YPD medium in each well. Cells were grown at 30 °C for 2 d to reach saturation without shaking; 500 µl of 50% glycerol was added to each well using a multi-channel pipette, then 1 ml of the mixture from each well was pooled in a container. The pooled cell culture was mixed well and aliquoted into 2-ml Eppendorf tubes, which were then stored at 80 °C for future fitness measurements.

Fitness measurement conditions. We measured clone fitness under four conditions: 1-, 2-, 3- and 5-d serial batch culture conditions (Fit1D, Fit2D, Fit3D and Fit5D, respectively). These four conditions are the same, except for the length of the growth cycle. From these, 1-, 2- and 5-d serial batch culture conditions are the same as Evo1D, Evo2D and Evo5D evolutionary conditions. Note that the fitness of Evo2D clones was measured in ref. [22]. Clones isolated from Evo1D, Evo5D and Evo1/5D were measured in this study and are analysed below. Note that all data reported in this section can be found in Supplementary Table 2.

Pre-culture. A tube of pooled cell culture was removed from freezing at −80 °C and thawed at room temperature. Pooled cell culture (1 ml) was inoculated into 15 ml fresh M3 medium contained in a 500-ml Delong flask and grown at 30 °C with shaking at 223 r.p.m. overnight for cell propagation. Overnight cell culture (400 µl) was inoculated into 100 ml fresh M3 medium (4×) and pre-cultured under standard conditions.

An ancestral clone carrying a restriction site in the barcode region was previously constructed and used to compete with evolved clones for fitness measurements[21]. This clone was streaked-out from freezer stock onto M3 agar plates and grown for 2 d until colonies became visible. A single colony was inoculated into 3 ml of M3 medium and grown for 48 h (30 °C roller drum). After saturation, 400 µl was used to inoculate pre-cultures (100 ml M3 medium in 500-ml Delong flasks, 223 r.p.m., 30 °C). As in the pooled cell culture, four pre-cultures were prepared.

The pooled pre-culture and ancestor pre-culture were acclimated for the same cycle length as that in the fitness measurement condition. For instance, pre-cultures were grown for 1 d before mixing and assay under the 1-d fitness measurement condition.

High-throughput competition. Fitness assays were conducted by mixing the pooled pre-culture with the ancestor pre-culture in a 1/9 ratio (time 0) and growing this mixed culture for four successive growth cycles (time points 1, 2, 3 and 4). In Fit1D, at the end of each cycle, 450 µl cell culture was inoculated into 100 ml fresh medium to start the next cycle. In Fit2D, Fit3D and Fit5D, at the end of each cycle 400 µl cell culture was inoculated. Cells reached a lower cell number after 1-d growth compared to after 2-, 3- and 5-d. Thus, we inoculated a larger volume to ensure that the number of cells inoculated was consistent across fitness measurement conditions. In addition, we inoculated 450 µl to ensure that the cell culture was close to saturation after 1-d growth and thus yielded sufficient cells for downstream analyses. Cells were collected at time 0, and at the end of each of the four growth cycles. A cell pellet from each sample was resuspended in 5 ml sorbitol solution (0.9 M sorbitol, 0.1 M Tris-HCL pH 7.5, 0.1 M EDTA pH 8.0), aliquoted into 2-ml Eppendorf tubes and stored at −20 °C. Three replicates were performed under each fitness assay condition. Genome extraction, barcode region amplification and Illumina sequencing were conducted for each sample.

Library preparation of high-throughput fitness assays. Genomic DNA was extracted using the following steps: (1) removal of collected cells from freezing at −20 °C and thawing at room temperature; (2) cells spun down and washed with water; (3) cells resuspended in 400 µl buffer (0.9 M sorbitol, 50 mM sodium phosphate pH 7.5, 240 µg ml^{-1} zymolase, 14 mM ß-mercaptoethanol) and incubated at 37 °C for 30 min; (4) addition of 40 µl 0.5 M EDTA and vortexing; (5) addition of 40 µl 10% SDS and vortexing; (6) addition of 56 µl 20 mg ml^{-1} proteinase K (Life Technologies, No. 25530–015), very brief vortexing and incubation at 65 °C for 30 min; (7) incubation of samples on ice for 5 min; (8) addition of 200 µl 5 M potassium acetate, shaking and incubation on ice for 30 min; (9) spinning for 10 min, transfer to supernatant in a new tube with 750 µl ispropanol and resting on ice for 5 min; (10) spinning down for 10 min and washing twice with 70% ethanol; (11) resuspension in 50 µl 10 mM Tris pH 7.5 (left on bench overnight if pellet not resuspended fully); and (12) addition of 0.5 µl 20 mg ml^{-1} RNase A and incubation at 65 °C for 30 min.

Two-step PCR was used to amplify the barcode region (see ref. [21] for primer details). The first-step PCR was conducted using 6 µg genomic DNA and separated into six 50 µl reactions:

- OneTaq 2× mix,150 µl
- Forward primer 5 uM, 3 µl
- Reverse primer 5 uM, 3 µl
- Template, 6 µg
- $MgCl_2$ 50 mM, 12 µl
- H_20, add up to 300 µl
- PCR programme for first-step PCR:
- 1 × 94 °C, 10 min
- 3 × 94 °C, 3 min
- 55 °C, 1 min
- 68 °C, 1 min
- 1 × 68 °C, 1 min
- 4 °C, infinite time

We then performed PCR clean-up following the QIAquick PCR purification protocol (six PCR reactions pooled into one column), with elution into 30 µl H_2O.

Second-step PCR was completed in one reaction using Herculase II fusion DNA polymerase (Agilent, No. 600677):

- Buffer, 10 µl
- dNTP 100 µM, 0.5 µl
- Herculase, 0.5 µl
- PE1 10 µM, 1.25 µl
- PE2 10 µM, 1.25 µl
- Template, 30 µl
- H_2O, 6.5 µl

PCR programme for second-step PCR:

- 1 × 98 °C, 2 min
- 20 × 98 °C, 10 s
- 69 °C, 20 s
- 72 °C, 30 s
- 1 × 72 °C, 1 min
- 4 °C infinite time

Fitness estimation. The number of DNA barcodes was tracked by Illumina sequencing (Illumina NextSeq), which was then used to estimate lineage frequency in the population as a whole, as previously described[21,22]. In this study, time points 0, 1, 2 and 3 were used for fitness estimates under Fit1D, Fit2D and Fit3D; time points 0, 1, 2, 3 and 4 were used for fitness estimates under Fit5D. The source code for computing these fitness estimates can be found at https://github.com/barcoding-bfa/fitness-assay-python. First, we input barcode counts to the script. After the first run, the script output barcodes that were likely to be neutral. During the second run, we input both the barcode counts and a list of neutral barcodes estimated from the first run. Fitness estimates from the second run were used for further analysis. Final fitness estimates were calculated by inverse variance weighting of estimates from all three replicates. Barcodes identified in these fitness assays were mapped back to barcodes identified in Metagrid. Thus, for each unique barcode, we know the fitness values under all fitness measurement conditions, its physical position in a 96-well plate in frozen stock, and the associated ploidy. Note that the physical position of each barcode is required for picking clones for genome-wide sequencing. In sum, 661 unique barcodes had confidently called ploidy and were successfully identified from our fitness assays. Out of these 661, 644 had high-quality fitness values under every fitness assay condition and were used for further analysis.

Classification of clones. The 644 lineages with high-quality fitness measurements were classified into four groups, based on their ploidy and fitness: neutral haploids, adaptive haploids, diploids presumed to have no additional adaptive mutations ('pure' diploids) and diploids with additional adaptive mutations (high-fitness

diploids; see ref. [22] for details). Briefly, adaptive haploids were defined as lineages with low probability ($P < 1e^{-3}$) of having log fitness of 0 or less in at least two conditions; high-fitness diploids were defined as diploid lineages with additional adaptive mutations that had low probability ($P < 1e^{-3}$) of having fitness less than the mean fitness of the diploid class in at least one condition. The mean fitness of the diploid population was calculated using inverse variance weighting. In total, 254 adaptive haploids, 66 high-fitness diploids, 218 neutral haploids and 106 pure diploids were characterized among clones isolated from Evo1D, Evo5D and Evo1/5D. See ref. [22] for classification of Evo2D clones.

Quantification of performance in growth phases. Fitness change per hour was used as the measurement of lineage performance in the different growth phases. Hourly respiration performance was calculated by subtracting Fit1D from Fit2D measurements and dividing by 24 h (because, compared to Fit1D, clones experienced 24 h of extra respiration in Fit2D while keeping the lag and fermentation phases roughly the same). Fit1D almost directly measures the performance in fermentation but contains ~4 h of respiration per transfer. Therefore, using the above estimates of hourly respiration performance, we subtracted the expected fitness change in the extra 4 h of respiration from Fit1D measurements. We then divided the difference by 16 h of fermentation to estimate hourly fermentation performance. Last, hourly stationary phase performance was calculated by subtracting Fit3D from Fit5D measurements and dividing the difference by 48 h of stationary phase. The same quantification was performed for Evo2D clones, using their fitness measured under 1-, 2-, 3- and 5-d serial transfer conditions[22]. See ref. [22] for statistical details.

Genome-wide sequencing and variant calling. *Genome-wide sequencing library preparation.* Clones selected for sequencing were grown in 500 µl YPD on 96-deep-well plates for 2 d at 30 °C without shaking, then 400 µl of cell culture was collected from each well for DNA extraction. Genomic DNA was prepared using the Invitrogen PureLink Pro 96 Genomic DNA Kit (No. K1821-04A) in a 96-well format. Libraries were constructed and multiplexed using Nextera technology with the protocol described in ref. [38]. Samples were sequenced with 2 × 150 Illumina NextSeq paired-end sequencing technology. We sequenced 179 adaptive haploids, 20 high-fitness diploids, eight neutral haploids and nine pure diploids, with average coverage >50 for both haploids and diploids. Note that only clones isolated from Evo1D, Evo5D and Evo1/5D were sequenced and analysed in this study and reported in this section. See refs. [21,22] for details on Evo2D clones.

FASTQ processing. The source code for variants calling and annotation can be found at https://github.com/liyuping927/DNAscope-variants-calling (sections 7.2–7.6).

For each sample, we received two fastq files, one for each read of the paired-end sequencing (fastqR1 and fastqR2). Using cutadapt v.1.16 (ref. [39]), we trimmed the first 10 bp of each read (-u 10), low-quality ends (-q 30) and any adaptor sequences (-a). After trimming, sequences of length <12 bp (–minimum-length 12) were discarded. Reads were mapped using bwa[40] to *Saccharomyces cerevisiae* S288C reference genome R64-1-1 (https://downloads.yeastgenome.org/sequence/S288C_reference/genome_releases/) and sorted using Sentieon Genomic Tools v.201711.02 (ref. [41]). Note that bwa used here is the default version incorporated in Sentieon Genomic Tools. Duplicates were removed using the sorted BAM file. Local realignment around indels was performed using the de-duped BAM file. Last, base quality score recalibration was performed using the realigned BAM file.

Single-nucleotide polymorphism and small indel variant calling. Single-nucleotide polymorphism (SNP) and small indel variants were called using the DNAscope algorithm (Sentieon Genomic Software) with the realigned BAM file and the output table of the base quality score recalibration. The parameter ploidy is assigned as 1 for haploids and 2 for diploids.

Structural variant calling. First, a DNAscope algorithm detected the break-end variant type (BND). The parameter ploidy was assigned as 1 for haploids and 2 for diploids. Second, SVSolver algorithm processed BND and output structural variants to a VCF file.

Copy number variant calling. First, recalibrated BAM files were created using previously generated aligned BAM files and quality score calibration tables. Second, the panel of normal (PON) was created using recalibrated BAM files. By changing the window size of the bed file, the window size used to call copy number variants (CNVs) was varied. Window sizes (200 bp and 10 kb) were applied in this study. The PON files were created only with the sequencing of haploids. Third, for each strain, the CNVs were called using the strain's recalibrated BAM file, the bed file and the PON file.

Variant annotation. VCF files from SNP and small indel variant calling and structural variant calling were further annotated using snpEff[42] (http://snpeff.sourceforge.net/download.html). For variants in coding regions, SNPSift was used to extract the first annotation of each variant, which is the annotation with the largest effect. For variants in non-coding regions, the nearest gene of each variant was extracted. Thus, the non-coding variants were annotated as either the upstream or downstream of the nearest genes.

Filtering SNPs, small indels and structural variants. First, mitochondrial variants were discarded. Second, background variants, present in all strains, were removed. Variants present in more than ten clones isolated from more than one evolutionary condition were also considered as background variants and discarded. Third, any variants in genes *FLO1* and *FLO9* were filtered out due to poor alignment in both genomic regions. Fourth, variants with a quality score <200 were filtered out. Note that if a variant was present in multiple clones, the alignment of this variant was manually checked regardless of its quality score and a decision was made based on all clones carrying this variant. Thus, a variant with a quality score <200 might not be filtered out if the same variant contained in other clones was shown to be authentic. Similarly, a variant with a quality score >200 might be filtered out if the same variant was shown to be bogus in other clones. Only six out of ~500 variants had a quality score <200. Last, by manually checking BAM files after alignment, variants within repetitive regions and regions with poor alignment were filtered out. In addition, if a variant was present in multiple clones and these clones carried a same-condition barcode, that variant was likely to have pre-existing mutations introduced during the barcoded population construction. These pre-existing mutations can be causative mutations and thus were retained in our analysis.

Filtering CNVs. Our DNA extraction and sequencing protocols resulted in an unevenly distributed and relatively low coverage of short chromosomes, including chromosomes I, III and VI. Thus, CNVs associated with these three chromosomes were not considered. For both haploids and diploids, CNVs generated with a 10-kb window size were used to identify large duplications and deletions, combined with visual inspection of coverage plots. These variants were further confirmed by CNVs generated with a 200-bp window size.

Detailed information on mutations. In total, 179 adaptive haploids, 20 high-fitness diploids, eight neutral haploids and nine pure diploids from Evo1D, Evo5D and Evo1/5D were sequenced in this study, with 163 adaptive haploids, 19 high-fitness diploids, eight neutral haploids and seven pure diploids having variants identified. All detailed information on these variants can be found in Supplementary Table 3.

Pre-existing mutations were identified as (1) those in the same gene that are the exact same alleles, and (2) clones carrying identical mutations in the same gene having the same condition barcodes. Thus, these pre-existing mutations were probably introduced during the construction of barcoded yeast populations. All eight sequenced neutral haploids and one out of nine sequenced pure diploids harbour chromosome IX duplication, suggesting that this duplication is not an adaptative event. Since lineages with chromosome IX duplications have different condition barcodes, it is likely that this duplication occurred independently during population construction. In this work, chromosome IX duplications are treated as pre-existing mutations. Note that even though the same pre-existing mutation appears in multiple clones, it is regarded as one independent adaptive event. Pre-existing mutations are not necessarily non-adaptive. For instance, despite pre-existing *SSK1* mutations, this mutation also occurred independently during evolution and thus is very likely to be adaptive. In addition, genes *LSM2*, *NUT2*, *TFB3*, *tL(GAG)G* and *VOA1* harbour both pre-existing mutations and those that occurred independently during evolution.

Lineages carrying mutations in genes *SSK1*, *SSK2* or *HOG1* are HOG pathway mutants. Lineages carrying mutations in Ras/PKA or TOR/Sch9 pathway genes are referred to as nutrient response pathway mutants in this work: *RAS2*, *GPB1*, *GPB2*, *PDE2*, *IRA1*, *CYR1*, *TFS1* and *YAK1* are involved in the Ras/PKA signalling pathway while *SCH9*, *TOR1*, *KOG1* and *MDS3* are involved in the TOR/Sch9 signalling pathway.

Recurrent mutations within genes or pathways are highly unlikely under neutral evolution and are a hallmark of adaptive mutations. Genes or pathways that were independently mutated five times or more are reported in Table 1, including the duplication of chromosome XI which appeared more than five times. The full list of genes that were independently hit more than once can be found in Supplementary Table 3. None of these multi-hit genes/pathways was mutated in the neutral haploids and pure diploids sequenced in this study. By contrast, these multi-hit genes/pathways were mutated in 118 out of 182 adaptive clones with identified variants (~65%). In addition, 79 out of 182 adaptive clones (~43%) harbour mutations in genes/pathways that were independently hit more than five times.

Three lineages carry mutations in coding regions of two genes listed in Table 1, offering an opportunity to study epistasis among these beneficial mutations. Specifically, these three lineages carry mutations in coding regions of *SXM1* and *SSK1*, *SXM1* and *HOG1* and *SXM1* and *CYR1*, respectively (Supplementary Fig. 4). These three lineages are not coloured in Fig. 3a–c. In addition, diploids with chromosome XI duplication and clones with *SSK2* mutations from Evo2D are not coloured in Fig. 3a–c. If a mutant harbours more than one mutation, providing that one, and only one, of the mutations is located in the genes listed in Table 1, it is classified as a mutant carrying mutations in those genes (Supplementary Fig. 1).

Identification and fitting of Pareto optimality fronts. The fermentation, respiration and stationary performance data of adaptive haploids and high-fitness diploids from Evo1D, Evo2D, Evo5D and Evo1/5D were used for the following analysis. The 'chull' function in R was used to identify the smallest set of points

(the convex set) that, when connected, enclosed the remaining points. By connecting the two points with the largest value on x or y, a line was formed. Out of the convex set, points either on or above this line were used to depict the Pareto front. Six, five and three points were identified to depict the Pareto front between the performances of fermentation and respiration, respiration and stationary, and fermentation and stationary phases, respectively.

With known points on Pareto fronts, regression was used looking for a curve that fit the front. The polynomial fit was evaluated using the Bayesian information criterion (BIC) and the adjusted R^2, where lower BIC and higher R^2 are considered a better fit. Both criteria include a penalty term for the number of parameters in the model, to avoid overfitting. Specifically, first- to third-degree polynomials were applied to the front between fermentation and respiration performance. We found the values of BIC to be −27, −40 and −43 and adjusted R^2 of 0.64, 0.96 and 0.97 for first-, second- and third-degree polynomial fit, respectively. The first-degree polynomial fit was rejected due to its poor BIC and adjusted R^2. Because the third-degree polynomial fit provides only a marginally better fit than the second, we opted for the simpler model. Specifically, the second-degree polynomial fit used is respiration = 0.047 + 0.746 × fermentation − 20.306 × fermentation^2. Similarly, first- to third-degree polynomials were applied to the front between respiration and stationary phase performance. BIC −33, −66 and −64 and adjusted R^2 0.81, 1.0 and 1.0 were observed for first-, second- and third-degree polynomial fit, respectively. Both BIC and adjusted R^2 values demonstrate that second-degree polynomial fit offers the best fit. Specifically, the second-degree polynomial fit respiration = 0.040 − 0.997 × stationary phase − 45.650 × (stationary phase)^2 was used. The second derivatives of both curves are negative, indicating that both are convex. Due to the small number of points on the front (three) between fermentation and stationary phase performance, we were unable to compare the first-degree polynomial fit to the second.

The inaccessible space is not generated by chance. We tested whether the observed Pareto fronts and evolutionary inaccessible spaces were generated by random chance. For each pair of performances, the evolutionary inaccessible space was defined as the empty space between the Pareto front (identified by the convex hull algorithm) and the upper limits of both performances. The null hypothesis assumes that a pair of performances are independent from each other.

The error of the fitness estimate is roughly Gaussian (see supplementary information in ref. [21]). Thus, for each fitness measurement, we resampled the fitness from a normal distribution with the estimated mean and standard deviation (resampling with error). Performances were recalculated from the resampled fitness. We then sampled the tested performances independently with replacement 504 times (the total number of adaptive clones from all four evolutionary conditions; resampled with permutation) from the recalculated performances, and calculated the amount of empty space under the null hypothesis.

We repeated the above test 1,000 times and calculated, under the null hypothesis, the chance of observing an empty space equal to or larger than that generated by our real data (Supplementary Fig. 2). For fermentation and respiration performance, none of the permutations had an empty space as large as that in the real data ($P < 0.001$). For respiration and stationary performance, four of the permutations had an empty space as large as that in the real data ($P = 0.004$). By contrast, for fermentation and stationary performance, when we sampled the marginal distributions the empty space we observed in the real data sits within the distribution of the empty spaces generated by the permutations; 761 of the permutations had an empty space larger than that observed in the real data ($P = 0.76$).

We then calculated the minimum number of clones needed to define the inaccessible space. By random sampling of current adaptive clones, we concluded that between 80 and 300 clones are required to confidently ($P \leq 0.01$) define the inaccessible space between fermentation and respiration performance, and between respiration and stationary phase performance, respectively.

Mathematical model used to calculate the probability of not sampling optimal types. *Equations.* By knowing the selection coefficient (s per generation) of a particular adaptive event, the bottleneck population size (N_b), the mutation rate (μ) and the effective variance of cell division per generation ($2c$), we can estimate the density distribution of establishment time (τ) of this adaptive event (equation 7 in supplementary information of ref. [20]). This density distribution represents, for a given time point, the probability that an adaptive event occurs and rises to c/s cells to avoid drift (see ref. [20] for details):

$$p(\tau)\mathrm{d}\tau = s/\Gamma(N_b \times \mu/c) \times \exp[-N_b \times \mu \times (s/c) \times \tau - \exp(-s \times \tau)]$$

After establishment, clones grow exponentially (cell number $n = c/s \times \exp[s \times (t-\tau)]$ with a given establishment time τ at a sampled time t). Thus, the frequency of the adaptive event (f) at a sampled time (t) can be estimated using the density distribution of establishment time:

$$f = \int_0^t \mathrm{d}\tau \times \frac{s}{\Gamma(N_b \times \mu/c)} \times \exp[-N_b \times \mu \times (s/c) \times \tau - \exp(-s \times \tau)] \times \frac{c}{N_b \times s} \times \exp[s \times (t-\tau)]$$

Lastly, by isolating I clones from the evolutionary experiment, we can estimate the probability of sampling this adaptive event:

$$\text{Probability (sampling this adaptive event)} = 1 - B(x = 0, \text{size} = I, p = f)$$

where $B(x = 0, \text{size} = I, p = f)$ represents a binomial sampling process—given the probability of sampling the adaptive event ($p = f$) and the number of clones sampled (size = I)—the probability of missing this adaptive clone ($x = 0$) during sampling. We use this binomial sampling because the number of adaptive clones sampled is not important in the calculation. Instead, whether or not the adaptive clone is sampled is more important.

Combining these three steps, we can calculate the probability to sample this particular adaptive event in one equation:

$$\text{Probability (sampling the adaptive event)} = \int_0^t \mathrm{d}\tau \times \frac{s}{\Gamma(N_b \times \mu/c)} \times \exp[-N_b \times \mu \times (s/c) \times \tau - \exp(-s \times \tau)] \times \left(1 - B\left[x = 0, \text{size} = I, p = \frac{c}{N_b \times s} \times \exp[s \times (t-\tau)]\right]\right)$$

Parameters. In our experiment, during each serial transfer cells are bottlenecked and then raised for $T \approx 8$ generations. As described in the supplementary information in ref. [20], the probability of the adaptive mutation arising during the first division of the cycle and surviving the bottleneck $\approx N_b \times \mu$. It is twice as likely to occur during the second division, but half as likely to survive the bottleneck, so the probability of a mutation entering at some point in the cycle and being present at a certain cell number once it is transferred to the next cycle is largely independent of where in the cycle it arises, always being proportional to $N_b \times \mu$ with $N_b = 7 \times 10^7$ (ref. [20]).

The variance ($2c$) in offspring number through the cycle (including Poisson noise of growth and bottleneck) is denoted as ~3.5 (supplementary information in ref. [20]). Assuming Poisson noise in each generation, the effective variance in offspring number per generation would be $2c = 3.5/T$ (ref. [20]).

Furthermore, ~90 neutral clones were isolated from Evo2D at generation 88 and sequenced in ref. [21]. Based on the number of mutations in their genomes, we estimated a mutation rate (μ) $\approx 9 \times 10^{-10}$ per base-pair per division.

Probability of not observing an optimal type with 1-bp mutational target size. Assume that there is 1 bp in the yeast genome that can be mutated to the optimal type. We want to estimate the probability of sampling such an adaptive event from our evolutionary conditions. We consider the conservative scenario where the optimal type can be generated only by a specific nucleic acid change. Thus, the mutation rate $\mu = 10 \times 10^{-10}/3 = 3 \times 10^{-10}$ will be used for the following calculation.

Take the optimal type in Evo2D as an example. Based on its performance in fermentation and respiration, we can estimate its fitness per growth cycle in Evo2D (s = 16 h × fermentation performance + 28 h × respiration performance = 2.56 per growth cycle). Because cells will grow up to eight generations per cycle, its fitness per generation is $s/8$. Two replicates were conducted for Evo2D, with 3,840 and 960 clones being isolated from replicates 1 and 2, respectively. Using the above parameters and equations, we can estimate that if such a 1-bp mutational target size exists, the probability of sampling this mutant from Evo2D replicates 1 and 2 is 0.82 and 0.80, respectively.

Similarly, the probability of observing a 1-bp optimal mutational event in Evo1D (s = 16 h × fermentation performance + 4 h × respiration performance = 1.49 per growth cycle), and in Evo5D (s = 40 h × respiration performance + 60 × stationary phase performance = 2.98 per growth cycle), is estimated. Note that the fitness of Evo5D optimal type is estimated by assuming a fermentation performance of zero. Because most adaptive clones gain benefits from performance, the fitness of Evo5D optimal type is very likely to be underestimated, providing a conservative calculation in our case. Two replicates were conducted for each evolutionary condition, with 800 clones being isolated from each replicate. With a 1-bp mutational target size, the probability of sampling this mutant from Evo1D replicate 1 or 2 is 0.39; the probability of sampling this mutant from Evo5D replicate 1 or 2 is 0.87.

Based on the above calculations, if the ancestral yeast can be mutated to maximize fermentation and respiration performance simultaneously by a single-step mutation, the probability of not observing such a mutant in both replicates of Evo1D and Evo2D will be $P = (1-0.39) \times (1-0.39) \times (1-0.82) \times (1-0.8) = 0.013$.

Similarly, if the ancestral yeast can be mutated to maximize respiration and stationary phase performance by a single-step mutation, the probability of not observing such a mutant in both replicates of Evo5D will be $P = (1-0.87) \times (1-0.87) = 0.017$.

Due to the difficulty in measuring fitness for Evo1/5D, the probability of not sampling such optimal types was not calculated. If Evo1/5D had been considered, the opportunity to miss such optimal types would have been even less than that estimated above.

A conservative estimate of the above probability. In our previous study[22], we noted an increase in fitness in one batch of measurements; nonetheless, fitness measurements across batches were highly correlated (Supplementary Fig. 5).

This batch of fitness measurements is used to infer fermentation and respiration performance among Evo2D adaptive clones in this study. Thus, the fitness estimate of the optimal type in the fermentation and respiration space may be both affected and inflated. Fitness measurements of Evo1D, Evo5D and Evo1/5D adaptive clones were conducted independently in a different batch. Therefore, these measurements have probably not suffered from such inflation.

However, to provide a conservative estimate, we corrected the estimated fitness of all optimal types by an inflation factor ($s\_correct = (s + 0.01)/1.472$; Supplementary Fig. 5) and generated corrected fitness estimates: s per cycle of Evo2D optimal type = 1.75, s per cycle of Evo1D optimal type = 1.02 and s per cycle of Evo5D optimal type = 2.04.

With corrected fitness estimates, the probability of sampling a single-mutation optimal type in Evo2D replicates 1 and 2 is 0.6 and 0.54, respectively; the probability of sampling a single-mutation optimal type in either replicate of Evo1D is 0.08; the probability of sampling a single-mutation optimal type in either replicate of Evo5D is 0.65.

Thus, if the ancestral yeast strain can be mutated to maximize fermentation and respiration performance simultaneously by a single-step mutation, the probability of not observing such a mutant in both replicates of Evo1D and Evo2D will be $P = (1 - 0.08) \times (1 - 0.08) \times (1 - 0.6) \times (1 - 0.54) = 0.156$.

If the ancestral yeast can be mutated to maximize respiration and stationary phase performance by a single-step mutation, the probability of not observing such a mutant in both replicates of Evo5D will be $P = (1 - 0.65) \times (1 - 0.65) = 0.123$, still strongly suggesting the absence of such a single-step mutation in the ancestral yeast genome.

Viability measurements. Two mutants carrying *FPK1* mutations (with one carrying an additional chromosome IX duplication) and two independent wild-type strains were cultured in monoculture for 5 d, for viability measurements. The number of viable cells forming colonies on plates was divided by the expected number measured by Coulter counter to calculate viability—the proportion of viable clones. Viability tests were conducted in two independent replicates with consistent results (Supplementary Table 4).

Reporting Summary. Further information on research design is available in the Nature Research Reporting Summary linked to this article.

Data availability

All sequencing data are deposited in Short Read Archive under Bioproject ID PRJNA515761. The remaining data are available in either the main text or the Supplementary tables. Figures 2 and 3 have associated raw data. All strains are readily available from the authors upon request.

Code availability

All code used in this manuscript is deposited in GitHub. The source code for computing these fitness estimates can be found at https://github.com/barcoding-bfa/fitness-assay-python. The source code for variant calling and annotation can be found at https://github.com/liyuping927/DNAscope-variants-calling.

Received: 7 May 2019; Accepted: 21 August 2019;
Published online: 14 October 2019

References

1. Loschiavo, S. R. Effect of oviposition sites on egg production and longevity of *Trogoderma parabile* (Coleoptera: Dermestidae)1. *Can. Entomol.* **100**, 86–89 (1968).
2. Tinkle, D. W. The concept of reproductive effort and its relation to the evolution of life histories of lizards. *Am. Nat.* **103**, 501–516 (1969).
3. Reznick, D. A., Bryga, H. & Endler, J. A. Experimentally induced life-history evolution in a natural population. *Nature* **346**, 357–359 (1990).
4. Stearns, S. C. *The Evolution of Life Histories* (Oxford Univ. Press, 1992).
5. Camargo, A., Sarroca, M. & Maneyro, R. Reproductive effort and the egg number vs. size trade-off in *Physalaemus* frogs (Anura: Leiuperidae). *Acta Oecologica* **34**, 163–171 (2008).
6. Cunningham, J. T. Degenerative mutations. *Nature* **130**, 203–204 (1932).
7. Wang, Y. et al. Contribution of both positive selection and relaxation of selective constraints to degeneration of flyability during geese domestication. *PLoS ONE* **12**, e0185328 (2017).
8. Darwin, C. *The Descent of Man, and Selection in Relation to Sex* (introduction by Bonner, J.T. & May, R.M.) (Princeton Univ. Press, 1981).
9. Shoval, O. et al. Evolutionary trade-offs, Pareto optimality, and the geometry of phenotype space. *Science* **336**, 1157–1160 (2012).
10. Tendler, A., Mayo, A. & Alon, U. Evolutionary tradeoffs, Pareto optimality and the morphology of ammonite shells. *BMC Syst. Biol.* **9**, 12 (2015).
11. Mooney, K. A., Halitschke, R., Kessler, A. & Agrawal, A. A. Evolutionary trade-offs in plants mediate the strength of trophic cascades. *Science* **327**, 1642–1644 (2010).
12. Fraebel, D. T. et al. Environment determines evolutionary trajectory in a constrained phenotypic space. *eLife* **6**, e24669 (2017).
13. Nidelet, T. & Kaltz, O. Direct and correlated responses to selection in a host–parasite system: testing for the emergence of genotype specificity. *Evol. Int. J. Org. Evol.* **61**, 1803–1811 (2007).
14. Buckling, A., Brockhurst, M. A., Travisano, M. & Rainey, P. B. Experimental adaptation to high and low quality environments under different scales of temporal variation. *J. Evol. Biol.* **20**, 296–300 (2007).
15. Bono, L. M., Smith, L. B., Pfennig, D. W. & Burch, C. L. The emergence of performance trade-offs during local adaptation: insights from experimental evolution. *Mol. Ecol.* **26**, 1720–1733 (2017).
16. McGee, L. W. et al. Synergistic pleiotropy overrides the costs of complexity in viral adaptation. *Genetics* **202**, 285–295 (2016).
17. Jasmin, J.-N. & Kassen, R. On the experimental evolution of specialization and diversity in heterogeneous environments. *Ecol. Lett.* **10**, 272–281 (2007).
18. Bennett, A. F. & Lenski, R. E. An experimental test of evolutionary trade-offs during temperature adaptation. *Proc. Natl Acad. Sci. USA* **104**, 8649–8654 (2007).
19. Satterwhite, R. S. & Cooper, T. F. Constraints on adaptation of *Escherichia coli* to mixed-resource environments increase over time. *Evolution* **69**, 2067–2078 (2015).
20. Levy, S. F. et al. Quantitative evolutionary dynamics using high-resolution lineage tracking. *Nature* **519**, 181–186 (2015).
21. Venkataram, S. et al. Development of a comprehensive genotype-to-fitness map of adaptation-driving mutations in yeast. *Cell* **166**, 1585–1596.e22 (2016).
22. Li, Y. et al. Hidden complexity of yeast adaptation under simple evolutionary conditions. *Curr. Biol.* **28**, 515–525.e6 (2018).
23. Seedorf, M. & Silver, P. A. Importin/karyopherin protein family members required for mRNA export from the nucleus. *Proc. Natl Acad. Sci. USA* **94**, 8590–8595 (1997).
24. Rosenblum, J. S., Pemberton, L. F. & Blobel, G. A nuclear import pathway for a protein involved in tRNA maturation. *J. Cell Biol.* **139**, 1655–1661 (1997).
25. Baccarini, L., Martínez-Montañés, F., Rossi, S., Proft, M. & Portela, P. PKA-chromatin association at stress responsive target genes from *Saccharomyces cerevisiae*. *Biochim. Biophys. Acta Gene Regul. Mech.* **1849**, 1329–1339 (2015).
26. Yona, A. H. et al. Chromosomal duplication is a transient evolutionary solution to stress. *Proc. Natl Acad. Sci. USA* **109**, 21010–21015 (2012).
27. Natesuntorn, W. et al. Genome-wide construction of a series of designed segmental aneuploids in *Saccharomyces cerevisiae*. *Sci. Rep.* **5**, 12510 (2015).
28. Sunshine, A. B. et al. The fitness consequences of aneuploidy are driven by condition-dependent gene effects. *PLoS Biol.* **13**, e1002155 (2015).
29. Garay, E. et al. High-resolution profiling of stationary-phase survival reveals yeast longevity factors and their genetic interactions. *PLoS Genet.* **10**, e1004168 (2014).
30. Levins, R. Theory of fitness in a heterogeneous environment. I. The fitness set and adaptive function. *Am. Nat.* **96**, 361–373 (1962).
31. Ehrlich, E., Kath, N. J. & Gaedke, U. The shape of a defense-growth trade-off governs seasonal trait dynamics in natural phytoplankton. Preprint at *bioRxiv* https://doi.org/10.1101/462622 (2018).
32. Jessup, C. M. & Bohannan, B. J. M. The shape of an ecological trade-off varies with environment. *Ecol. Lett.* **11**, 947–959 (2008).
33. Maharjan, R. et al. The form of a trade-off determines the response to competition. *Ecol. Lett.* **16**, 1267–1276 (2013).
34. Roff, D. A. & Fairbairn, D. J. The evolution of trade-offs: where are we? *J. Evol. Biol.* **20**, 433–447 (2007).
35. Yi, X. & Dean, A. M. Phenotypic plasticity as an adaptation to a functional trade-off. *eLife* **5**, e19307 (2016).
36. Sexton, J. P., Montiel, J., Shay, J. E., Stephens, M. R. & Slatyer, R. A. Evolution of ecological niche breadth. *Annu. Rev. Ecol. Evol. Syst.* **48**, 183–206 (2017).
37. Zhao, L., Liu, Z., Levy, S. F. & Wu, S. Bartender: a fast and accurate clustering algorithm to count barcode reads. *Bioinformatics* **34**, 739–747 (2018).
38. Kryazhimskiy, S., Rice, D. P., Jerison, E. R. & Desai, M. M. Global epistasis makes adaptation predictable despite sequence-level stochasticity. *Science* **344**, 1519–1522 (2014).
39. Martin, M. Cutadapt removes adapter sequences from high-throughput sequencing reads. *EMBnet. J.* **17**, 10–12 (2011).
40. Li, H. Aligning sequence reads, clone sequences and assembly contigs with BWA-MEM. Preprint at https://arxiv.org/abs/1303.3997 (2013).
41. Freed, D. N., Aldana, R., Weber, J. A. & Edwards, J. S. The Sentieon genomics tools – a fast and accurate solution to variant calling from next-generation sequence data. Preprint at *bioRxiv* https://doi.org/10.1101/115717 (2017).
42. Cingolani, P. et al. A program for annotating and predicting the effects of single nucleotide polymorphisms, SnpEff. *Fly (Austin)* **6**, 80–92 (2012).

Acknowledgements

We thank A. Agarwala, G. Kinsler, C. McFarland and D. Fisher for discussions. We thank J. Blundell, K. Geiler-Samerotte, O. Kolodny, S. Kryazhimskiy, C. Li, F.

Rosenzweig and S. Venkataram for comments on the manuscript. We thank all members in the Sherlock and Petrov labs for helpful suggestions. Y.L. is supported by the Stanford Center for Computational, Human and Evolutionary Genomics Predoctoral Fellowship. The work was supported by NIH grants (nos. R01 GM110275 and R35 GM131824), a NASA grant (no. NNX17AG79G to G.S.) and a NIH grant (no. R35GM118165 to D.A.P.).

Author contributions

Y.L., G.S. and D.A.P. were responsible for conceptualization. Y.L. performed the methodology. Formal analysis was carried out by Y.L. Investigation was performed by Y.L. Y.L. wrote the original draft. Y.L., D.A.P. and G.S. undertook the writing, review and editing. Supervision was carried out by D.A.P. and G.S.

Competing interests

The authors declare no competing interests.

Additional information

Supplementary information is available for this paper at https://doi.org/10.1038/s41559-019-0993-0.

Correspondence and requests for materials should be addressed to D.A.P. or G.S.

Reprints and permissions information is available at www.nature.com/reprints.

Publisher's note Springer Nature remains neutral with regard to jurisdictional claims in published maps and institutional affiliations.

nature research

Corresponding author(s): Dmitri Petrov and Gavin Sherlock

Last updated by author(s): 8/12/2019

Reporting Summary

Nature Research wishes to improve the reproducibility of the work that we publish. This form provides structure for consistency and transparency in reporting. For further information on Nature Research policies, see Authors & Referees and the Editorial Policy Checklist.

Statistics

For all statistical analyses, confirm that the following items are present in the figure legend, table legend, main text, or Methods section.

n/a	Confirmed	
☐	☒	The exact sample size (*n*) for each experimental group/condition, given as a discrete number and unit of measurement
☐	☒	A statement on whether measurements were taken from distinct samples or whether the same sample was measured repeatedly
☐	☒	The statistical test(s) used AND whether they are one- or two-sided *Only common tests should be described solely by name; describe more complex techniques in the Methods section.*
☒	☐	A description of all covariates tested
☐	☒	A description of any assumptions or corrections, such as tests of normality and adjustment for multiple comparisons
☐	☒	A full description of the statistical parameters including central tendency (e.g. means) or other basic estimates (e.g. regression coefficient) AND variation (e.g. standard deviation) or associated estimates of uncertainty (e.g. confidence intervals)
☐	☒	For null hypothesis testing, the test statistic (e.g. *F*, *t*, *r*) with confidence intervals, effect sizes, degrees of freedom and *P* value noted *Give P values as exact values whenever suitable.*
☒	☐	For Bayesian analysis, information on the choice of priors and Markov chain Monte Carlo settings
☒	☐	For hierarchical and complex designs, identification of the appropriate level for tests and full reporting of outcomes
☒	☐	Estimates of effect sizes (e.g. Cohen's *d*, Pearson's *r*), indicating how they were calculated

Our web collection on statistics for biologists contains articles on many of the points above.

Software and code

Policy information about availability of computer code

Data collection	No software was used
Data analysis	Source code for computing fitness estimates: https://github.com/barcodingbfa/fitness-assay-python Source code for variants calling: https://github.com/liyuping927/DNAscope-variants-calling

For manuscripts utilizing custom algorithms or software that are central to the research but not yet described in published literature, software must be made available to editors/reviewers. We strongly encourage code deposition in a community repository (e.g. GitHub). See the Nature Research guidelines for submitting code & software for further information.

Data

Policy information about availability of data

All manuscripts must include a data availability statement. This statement should provide the following information, where applicable:

- Accession codes, unique identifiers, or web links for publicly available datasets
- A list of figures that have associated raw data
- A description of any restrictions on data availability

All sequencing data are deposited in Short Read Archive under Bioproject ID PRJNA515761. The rest of data is available in the main text or the supplementary tables. Figure 2 and 3 have associated raw data.

Field-specific reporting

Please select the one below that is the best fit for your research. If you are not sure, read the appropriate sections before making your selection.

☐ Life sciences ☐ Behavioural & social sciences ☒ Ecological, evolutionary & environmental sciences

For a reference copy of the document with all sections, see nature.com/documents/nr-reporting-summary-flat.pdf

Ecological, evolutionary & environmental sciences study design

All studies must disclose on these points even when the disclosure is negative.

Study description	We evolved barcoded yeast populations under well-controlled laboratory conditions, isolated adaptive clones from each evolutionary condition and characterized the genetic basis and performance of these clones.
Research sample	Barcoded yeast cells (Saccharomyces cerevisiae)
Sampling strategy	Standard serial batch culture sampling (See Methods for details)
Data collection	Yuping Li collected data from experimental evolution experiments and fitness measurement experiments
Timing and spatial scale	Sampled based on experimental design
Data exclusions	For fitness measurements, time points with a low sequencing coverage were discarded.
Reproducibility	Evolution were conducted in two replicates. Fitness measurements were conducted in three replicates. Data are reproducible among replicates.
Randomization	Sample randomization is not applicable to this study.
Blinding	Sample blinding is not applicable to this study.

Did the study involve field work? ☐ Yes ☒ No

Reporting for specific materials, systems and methods

We require information from authors about some types of materials, experimental systems and methods used in many studies. Here, indicate whether each material, system or method listed is relevant to your study. If you are not sure if a list item applies to your research, read the appropriate section before selecting a response.

Materials & experimental systems

n/a	Involved in the study
☒	☐ Antibodies
☒	☐ Eukaryotic cell lines
☒	☐ Palaeontology
☒	☐ Animals and other organisms
☒	☐ Human research participants
☒	☐ Clinical data

Methods

n/a	Involved in the study
☒	☐ ChIP-seq
☒	☐ Flow cytometry
☒	☐ MRI-based neuroimaging